Research Article | Vol. 33, No. 3 / 10 Feb 2025 / Optics Express 6105

Optics EXPRESS

# Blue-pumped photorefractive optical transient detection with low-power femtosecond laser pulses

SUKEERT,[1] S. CHAITANYA KUMAR,[2] P. G. SCHUNEMANN,[3] M. EBRAHIM-ZADEH,[1,4] AND A. ESTEBAN-MARTÍN[5,*]

[1]*ICFO—Institut de Ciències Fotòniques, The Barcelona Institute of Science and Technology, 08860 Castelldefels (Barcelona), Spain*
[2]*Tata Institute of Fundamental Research Hyderabad, 36/P Gopanpally, Hyderabad 500046, Telangana, India*
[3]*BAE Systems Inc., MER15-1813, P.O. Box 868, Nashua, New Hampshire 03061-0868, USA*
[4]*Institució Catalana de Recerca i Estudis Avançats (ICREA), Passeig Lluís Companys 23, Barcelona 08010, Spain*
[5]*Departament d'Òptica i Optometria i Ciències de la Visió, Universitat de València, Dr. Moliner 50, 46100-Burjassot, Spain*
[*]*adolfo.esteban@uv.es*

**Abstract:** We demonstrate optical transient detection (OTD) via photorefractive two-wave mixing using visible femtosecond pulses. This technique utilizes a nonlinear crystal to perform OTD directly in the blue spectrum by employing second-harmonic generation (SHG) of high-repetition-rate infrared pulses. The approach enables measurement of phase variations in dynamic signals by using conventional Si-based detectors, while effectively minimizing stationary background fluctuations. Results show a correlation between input phases and output intensities, and condition for enhanced phase sensitivity under weak phase modulation. Additionally, we demonstrate that synchronization of blue pulses results in low-average-power requirement for OTD using a single nonlinear crystal.



## 1. Introduction

Phase measurement plays a crucial role in optical systems, enabling the detection of minute changes in the properties of light, such as wavefront distortions, refractive index variations, or motion-induced shifts. In many applications, such as microscopy, material characterization, and fluid dynamics, accurate phase measurement is essential for extracting information about an object or a process that is not easily detectable through intensity alone. Interferometry, a technique that compares the phase difference between two or more light waves, is established as one of the most precise methods for measuring these changes. However, traditional interferometers are often sensitive to environmental fluctuations such as temperature variations, mechanical vibrations, or air turbulence, which can degrade measurement accuracy. To overcome these challenges, adaptive interferometers, which are capable of compensating for slow environmental perturbations, have been developed, providing more accurate and reliable phase measurements.

One such adaptive approach is based on two-wave mixing (TWM) in photorefractive crystals, which offers a particularly attractive solution for optical phase detection with background suppression. TWM in photorefractive crystals presents a promising method for interferometry, particularly for optical phase detection with enhanced background suppression. This is due to the inherent spatial and temporal adaptability of photorefractive systems. The suppression of background signals significantly increases contrast, allowing for improved visualization as well as more precise retrieval of both intensity and phase information. In interferometers that utilize photorefractive crystals, a dynamic refractive index grating is formed within the crystal through

#546473 https://doi.org/10.1364/OE.546473
Journal © 2025 Received 29 Oct 2024; revised 22 Jan 2025; accepted 26 Jan 2025; published 6 Feb 2025

Optics EXPRESS

the interference pattern generated by the TWM process. In this light-matter interaction, both the signal and pump beams not only contribute to the formation of this grating but also pass through and diffract from it, facilitating a process known as beam coupling [1–3]. This allows the system to act as an adaptive interferometer, where the grating continuously adjusts to compensate for slow, undesirable fluctuations in the wavefront of the beams. In this context, photorefractive adaptive interferometers are able to compensate for these external perturbations, making them highly suitable for maintaining consistent phase measurements over time. However, the dynamic nature of the grating is limited to slower variations, meaning that it cannot keep pace with rapid phase changes. As a result, such fast phase shifts are converted into intensity modulation at the output, making it possible to detect changes that occur at high speeds.

OTD based on TWM process using continuous-wave (cw) visible lasers, has been employed in imaging systems designed for transient detection imaging (TDI), a technique sometimes referred to as optical novelty filtering. Early demonstrations of photorefractive TWM-based TDI systems were conducted by Cronin-Golomb et al. [4], and their theoretical foundation was later expanded by Anderson and Feinberg [5]. Such optical novelty filters have found widespread applications, including transient detection microscopy [6], particle velocimetry [7], and the analysis of microflow dynamics [8]. Additionally, they have been employed for real-time measurement of phase changes induced by moving objects, as reported by C. Denz et at. [9–11]. Recent advancements have also allowed precise measurements of transient output phase in imaging devices, and how these relate to input phase changes [12]. These breakthroughs were made possible using off-axis interferometry, a technique that enables phase measurement by complex-field recovery. Regarding detection in single-spot photodetector systems, some previous works have deployed photorefractive adaptive interferometers. For instance, near-infrared cw lasers in adaptive interferometers with semiconductor materials [13–21] as well as visible lasers with liquid crystals [22] have been demonstrated for applications in laser ultrasonics. Moreover, protein detection has been reported in photorefractive quantum-well device which performs adaptive interferometry of protein on a BioCD [23]. As such, adaptive interferometers based on photorefractive TWM have become practical tools, where real-time phase monitoring and high-speed optical detection are critical.

Nevertheless, OTD with ultrashort pulses in the visible has not been explored to date. Optical sources capable of providing high-repetition-rate femtosecond pulses in the visible spectrum are of interest for variety of research fields such as time-domain spectroscopy, optical microscopy, frequency metrology, quantum optics, and biophotonics. The most direct route to the generation of such pulses is external frequency doubling of Kerr-lens mode-locked (KLM) Ti:sapphire laser, which can provide practical average powers over 350–500 nm spectral range [24]. Other practical sources are optical parametric oscillators, which provide broad wavelength tunability [25]. Therefore, the combination of ultrafast lasers with OTD foresees several new possibilities. On the one hand, it enables frequency conversion processes providing wavelength flexibility for both sampling and detection, such as up-conversion [26–30]. On the other hand, the use of delayed femtosecond pulses might allow combining OTD with optical coherence tomography and reflectometry [31].

In 2023, we demonstrated photorefractive OTD with femtosecond laser pulses by using TWM in the near-infrared [32]. However, the process was not very efficient and an architecture of two photorefractive crystals in tandem was required. Another drawback was that a relatively high signal average power of 100 mW was necessary to perform OTD detection, primarily due to the requirement of up-conversion of the near-infrared signal into the visible for detection.

In this new proof-of-concept demonstration, we report OTD in single-spot photodetector directly using visible femtosecond pulses from a mode-locked Ti:sapphire laser, for the first time. The high peak power of the ultrashort fundamental infrared pulses from a mode-locked Ti:sapphire laser enables second-harmonic-generation (SHG) into the blue spectral range, thus

Optics EXPRESS

allowing detection of output transient signals directly in the visible. Moreover, we investigate the OTD output phase in the visible and its relation to the input signal-phase changes. The implementation of blue-pumped transient signal detection and analysis opens up avenues for exploiting new architectures for the technique, while taking advantage of the fast and low-noise off-the-shelf detectors available in the visible. It should be noted that while here we demonstrate visible OTD in a photodetector, the approach could also be extended to imaging.

As described above, several demonstrations have been reported based on the OTD concept, but mostly in the visible range and using cw lasers. Demonstration of refractive index grating formation by TWM using ultrashort pulses has been reported for signal amplification in some photorefractive materials such as $BaTiO_3$ and $Sn_2P_2S_6$ [33–41]. However, adaptive signal suppression and phase detection using visible OTD, with both grating formation and detection obtained directly in visible wavelength, has not been previously demonstrated.

## 2. Theoretical background

As a starting point, let us provide a brief overview of the theoretical framework for two-wave mixing in the context of transient detection within photorefractive materials. Additionally, we will present the mathematical formalism that describes the relationship between phase variations in the input signal and the corresponding intensity variations in the output. The photorefractive effect is a phenomenon in which the local index of refraction of a material is modified by a structured light beam with spatial variations of intensity. Basically, two beams that interfere in a photorefractive crystal can create an index grating, where the grating is created by the Pockels effect. In materials dominated by diffusion-type charge transport, the index grating is shifted from the intensity pattern by $\pi/2$ and energy transfer from one beam to the other may occur, depending on the orientation of the c + axis of the crystal. As a result of the interaction of the beams with the index grating, one beam is attenuated and the other is amplified. For OTD, the c + axis is reversed by 180° in order to obtain signal suppression. Thus, if the signal changes more quickly than the response time of the photorefractive grating (ranging from seconds to microseconds), the transmitted beam passing through the crystal will generate a signal that reflects the changes in the original signal. We must indicate that theory of OTD under full signal suppression is described in detail in [12], but in the current experiment reported here, we have not reached full suppression but strong attenuation, up to 60% of the input signal intensity. Adaptation of the theory to our experimental condition, including the use of ultrafast mode-locked laser pulses, can be found in [32], where certain background signal intensity, $I^0$, is present, and OTD intensities are given by

$$I^{\mathrm{OTD}} = I^{out} - I^0 = 4I^{\mathrm{ref}}\sin^2\left(\frac{\Delta\varphi}{2}\right), \tag{1}$$

where $I^{out}$ is the signal output intensity and $\Delta\phi$ is the input signal-phase shift. $I^{\mathrm{ref}}$ is a coefficient which can be determined experimentally by means of a fit to the dependence of $I^{\mathrm{OTD}}$ on$\Delta\varphi$. This method is the basis of the conventional approach of inferring the input phase change from intensity measurements [10,32].

However, an important difference with respect to cw illumination is the effect of synchronously overlapping pump and signal pulses inside the crystal. When pulses are in synchronization, the illumination behaves as cw. Any relative delay will give rise to modifications in the intensity pattern, which clearly results in a decrease in intensity. Moreover, it is worthwhile to remark that if the peak intensity is small enough to ignore two-photon absorption, the OTD theory under cw illumination is applicable to our experiments. As we will see in Section 3, the overlapping beams in the photorefractive crystal are not focused, thus ensuring that no additional nonlinear effects are present.

Optics EXPRESS

Finally, regarding the characterization of our system, we define the suppression contrast, as the ratio of the signal output intensities with and without TWM, as follows

$$\gamma^{\text{supp}} = 100\ (I^{\text{free}} - I^{0})/I^{\text{free}}, \tag{2}$$

where $I^{\text{free}}$ is signal intensity directly transmitted through the photorefractive crystal in the absence of TWM. As we will see in Section 5, the suppression contrast depends on the average pump power and the highest values are achieved when the pulses are synchronized.

A useful parameter to measure the signal amplification in TWM is the gain, which is defined as [1]:

$$g = \frac{I^{0}}{I^{in}} = \frac{(1+m)}{1+me^{-\Gamma l_c}} e^{-\alpha l_c}, \tag{3}$$

where $\Gamma$ is the exponential coupling gain, $\alpha$ is the absorption coefficient, $l_c$ is the crystal length, and $m = I^{pump}/I^{in}$ is the ratio between the input pump, $I^{pump}$, and the input signal, $I^{in}$.

The signal suppression contrast formula used in the manuscript, $\gamma^{\text{supp}}$, can be written in terms of the gain coefficient as follows:

$$\gamma^{\text{supp}} = 100(T - g)/T, \tag{4}$$

where we have identified $I^{\text{free}} = TI^{in}$, $I^{0} = gI^{in}$, and $T = e^{-\alpha l_c}$ is accounting for absorption losses and has been introduced to simplify notation.

Accordingly, the exponential coupling gain will be:

$$\Gamma = -\frac{1}{l_c} \ln\left[\left(\frac{1+m}{m}\right)\frac{T}{g} - \frac{1}{m}\right]. \tag{5}$$

Note that the sign of the exponential coupling gain is negative, in agreement with the fact that the signal intensity is in suppression geometry (energy flows from signal to pump).

## 3. Experimental setup

The schematic of the experimental setup for the blue-pumped femtosecond OTD system is shown in Fig. 1. The pump source is a Kerr-lens mode-locked (KLM) Ti:sapphire laser (Coherent, Mira 900) at 805 nm, providing up to 800 mW average power at 76 MHz pulse repetition rate. After an optical isolator to prevent back-reflections into the laser, the pulses have a duration of ~150 fs. The polarization of the laser beam is controlled using a half-wave plate. The first part of the experimental setup includes the up-conversion stage. Frequency doubling of the laser beam is achieved in a single pass through a second-order nonlinear crystal (C1), which is a $BiB_3O_6$ (BiBO) sample with $3 \times 6$ mm$^2$ aperture and 4.6 mm length. The crystal is cut for collinear critical type I ($e + e \rightarrow o$) interaction in the optical $yz$ plane ($\phi = 90°$) at an internal angle of $\theta \cong 152.8°$ at normal incidence. This geometry yields a maximum theoretical effective nonlinear coefficient of $d_{\text{eff}} \cong 3.3$pm/V [24,42]. The input and output faces of the crystal are anti-reflection coated for 790-850 nm and 395-425 nm, respectively. The BiBO crystal is deployed to receive the input in $o$-polarization with respect to the optical setup, corresponding to an $e$-wave with respect to the BiBO crystal axis, to yield optimum phase-matching. In this scheme, the up-converted blue beam is already generated with the extraordinary polarization with respect to the optical setup and the photorefractive crystal axis for the TWM process. The fundamental beam from the laser is focused onto the BiBO crystal with a lens L1 ($f' = 75$ mm, infrared AR - coated), and the blue light is collimated by a lens L2 ($f' = 75$ mm, visible AR - coated). The infrared and second harmonic blue beams are split by means of a harmonic separator (HS) designed to reflect 400 nm at 45°, and transmit the fundamental. A second HS is deployed to ensure that no fundamental is present.

Optics EXPRESS

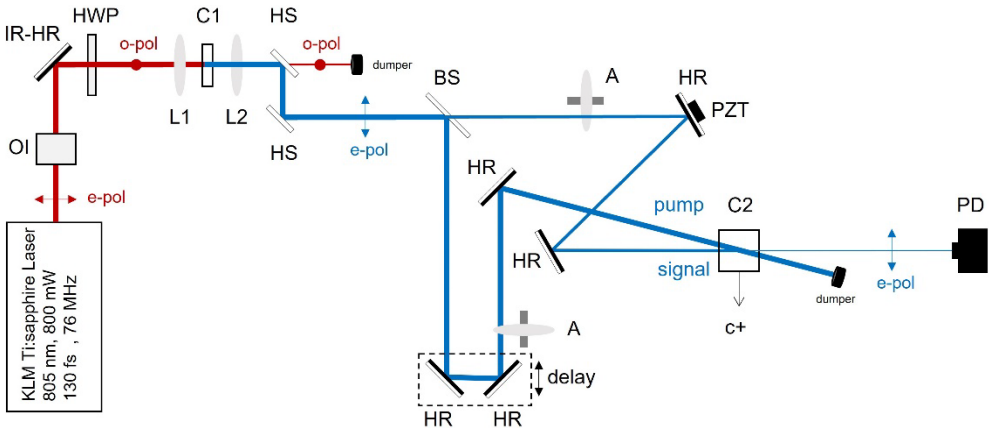


**Fig. 1.** Experimental setup for blue-pumped femtosecond OTD. The mean output beam from the laser is up-converted via SHG in a BiBO (C1) crystal. Signal and pump interact at the $BaTiO_3$ (C2) photorefractive crystal via TWM. OI: optical isolator. HWP: half-wave plate. BS: beam splitter. IR-HR: IR high-reflector. HR: blue high-reflector. HS: harmonic separator. PZT: piezo-electric transducer. A: attenuator. L1-L2: lenses. PD: photodetector. e-pol: extraordinary polarization (horizontal). *o*-pol: ordinary polarization (vertical).

The blue laser beam is split into a weak signal and a strong pump beam using a Thorlabs BSW10 50:50 beam-splitter (BS). Signal and pump optical attenuators (A) are used for control and optimization of pump/signal ratios. The signal and pump beams intersect at the second nonlinear crystal (C2), a barium titanate ($BaTiO_3$) photorefractive crystal (BAE Systems), of $5.23 \times 6.67$ mm$^2$ aperture and 7 mm length. The angle between pump and signal was set at 20°, and thus, the grating period was of the order of 0.5 microns. The $c^+$-axis of the crystal is oriented in order to enable energy transfer from signal to pump under steady-state operation. It should be noted that we also used a 0.01 wt% $CeO_2$-doped strontium barium niobate (SBN:61) photorefractive crystal (Altechna, $5 \times 5 \times 5$ mm$^3$) available in our laboratory, but observed no evidence of grating formation in the blue. Using the setup with $BaTiO_3$, we obtain a final output beam which is stable, suppressed and provides visible radiation which can be detected when the signal beam phase changes. This system forms the photorefractive adaptive interferometer arranged for visible OTD. In order to provide temporal variations with precise phase change, the signal beam is reflected with a high reflector (HR) mounted on a piezo-electric transducer (PZT) which is connected to a high-voltage amplifier and a function generator (Rigol, DG822).

The output beam is directed to a Si photodetector, Thorlabs DET10A2 (200 - 1100 nm, 1 ns rise time, 0.8 mm$^2$). Owing to the fast photodetector and a customizable function generator, we were able to explore the detection of various signal-phase changes and fully characterize the system, as described in the next section.

## 4. Experimental procedure

In the second harmonic process in BiBO in the first stage of the experiment, we were able to obtain ~350 mW of average power in the blue for an input fundamental power of 780 mW, at a conversion efficiency of ~45%. In the second stage, the experimental procedure requires preparation of the photorefractive adaptive interferometer into a suppression state. To achieve that, we perform TWM in the $BaTiO_3$ photorefractive crystal to obtain a significant level of background suppression and stability to perturbations. Specifically, we mix both signal and pump in the photorefractive crystal. The two pulses are synchronized using a delay line to achieve overlap in space and time in the crystal. The synchronization range for our mode-locked

Optics EXPRESS

pulses is measured to be ~150 μm, corresponding to pulse durations of the order of 500 fs for the blue pulses, as expected from the typical pulse broadening in SHG using BiBO crystal [42]. Therefore, we monitor the output on photodetector and scan the pump delay line until we observe the onset of suppression, and then, leave the system evolving while the photorefractive grating is created. Small adjustments of crystals orientations and realignment of pump beam and the delay line for spatial and temporal overlap are required in an iterative process to enhance the level of suppression. Figure 2 shows an example of the temporal dynamic of grating formation in the $BaTiO_3$ crystal for output suppression under illumination with blue femtosecond pulses. In this procedure, when we release and synchronize the pump for TWM in the crystal, a grating is created in about 10s. When the system is ready in the suppressed configuration, fast fluctuations are immediately revealed, as a result of the phase-sensitive interferometric process owing to TWM. As one can see from the inset of Fig. 2, the average suppression level is 77 m*V*, with a standard deviation (*std*) of 0.2 mV, providing a final state with a 60% signal suppression. Moreover, the experimental procedure to demonstrate signal-phase detection consists of applying different signal phase variations on the input signal and analyzing the intensity outputs. As shown in the experimental setup (see Fig. 1) the signal beam is reflected onto a HR mirror mounted on PZT, and a function generator is arranged to provide different sort of signals, including ramps as well as square pulses. Ramps are used to infer the response function of our system for the entire phase range from 0 to π in a single-shot measurement. Additionally, square pulses with different amplitudes are employed to inspect OTD under discrete phase variations on the blue optical beam. In next section, we present main results making use of the described experimental procedures.

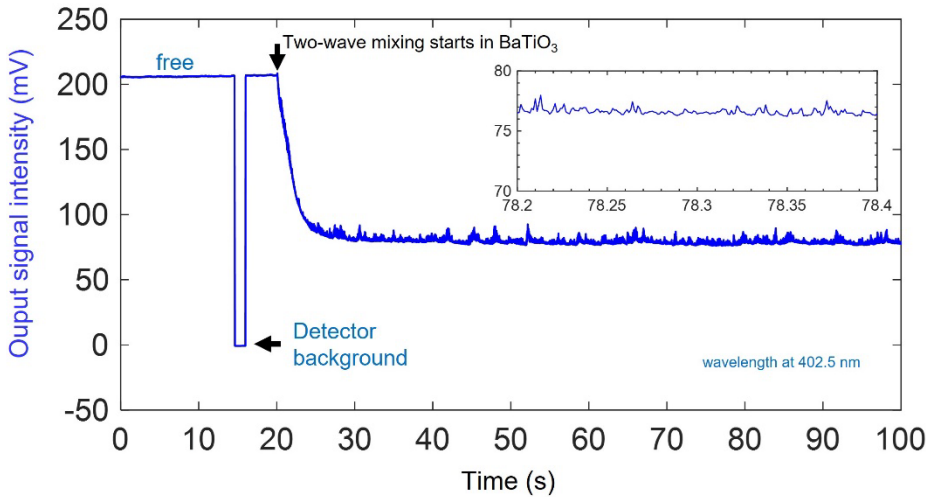


**Fig. 2.** Example of femtosecond TWM grating formation for intensity suppression in the blue. The curve includes the initial intensity level (free), the background level of the photodetector, TWM starting point, and evolution of suppression towards its final state. The input signal and pump powers are 1 mW and 120 mW, respectively. The inset shows a zoom of the output signal after grating formation. Oscilloscope acquisition is set at 1 kS/s for 100 k points.

## 5. Results

As a starting point, we measure the performance of our experimental setup in terms of output signal suppression. Figure 3 presents the suppression contrast, $\gamma^{supp}$, described by Eq. (2), as a function of the average pump power. As one can see from the plot, the suppression contrast

Optics EXPRESS

seems to follow a quadratic behavior at pump powers from 1 to 10 mW, but then continues to grow from 12% to a maximum value of 60% for the available 120 mW of pump power.

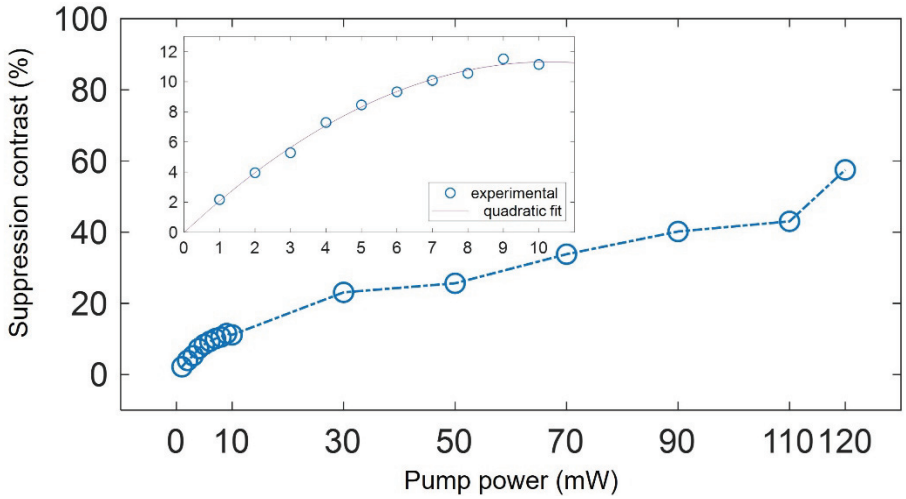


**Fig. 3.** Signal output suppression contrast, $\gamma^{\text{supp}}$, Eq. (2), depending on average pump power. The input signal average power was only 1 mW. Plot contains experimental values and dashed line is added as guide to the eye. The inset presents a zoom of the plot for low pump powers, including the quadratic fit with a correlation factor $R = 0.996$.

Interestingly, $\gamma^{supp}$ shows an increasing trend, reaching higher values than expected due to the purely quadratic behavior obtained (see inset of Fig. 3). This might be due to some beam change that affects the TWM process when average pump power on the photorefractive crystal increases, providing an additional decrease in the signal background. Notably, the performance of this system, in terms of low input signal power and high contrast suppression, is superior than previous work based on tandem crystals pumped in the infrared [32].

In this work, with a single crystal, the maximum suppression contrast is $\gamma_{max}^{supp} = 60\%$, which will correspond to a gain value $g = T\left(1 - \left(\frac{\gamma_{max}^{supp}}{100}\right)\right) = 0.0243\,(\sim 2.4\%)$, according to Eq. (4), when considering $T = 0.0608\,(\sim 6\%)$. Note that $T$ is inferred from the absorption measurement $\alpha = 4\ cm^{-1}$, obtained for the extraordinary polarization required for the TWM process. Accordingly, for a beam ratio of $m = 120$, the exponential coupling gain, given by Eq. (5), will be $\Gamma = -1,32\,cm^{-1}$.

It is worthwhile to point out that the sign of the exponential coupling gain is negative and, consequently, the gain value is lower than 1, in agreement with the fact that the signal intensity is in suppression mode.

Figure 4 displays the measured OTD output signals for an input signal with a step-like phase variation, set by applying a dc-voltage to the PZT mirror, with a very fast rise time of 5 ns. As soon as the phase change is applied on the input blue beam, the output shows a sharp increase in intensity, then gradually decays back towards the steady state again. The measured full-width at half-maximum (FWHM) is 150 ms, whereas the $1/e^2$ pulse duration decay is 400 ms, which we may consider as the response time of our system.

In order to characterize the performance of our system for phase measurements, we arrange a set of intensity measurements for different values of phase changes by applying a ramp on the blue signal beam. Figure 5 displays the temporal measurements of the OTD output signal as well as the applied linear phase variations ranging from 0 to $2\pi$. The ramp was applied for a duration of 25 ms, which is much shorter than the response time of our photorefractive material

Optics EXPRESS

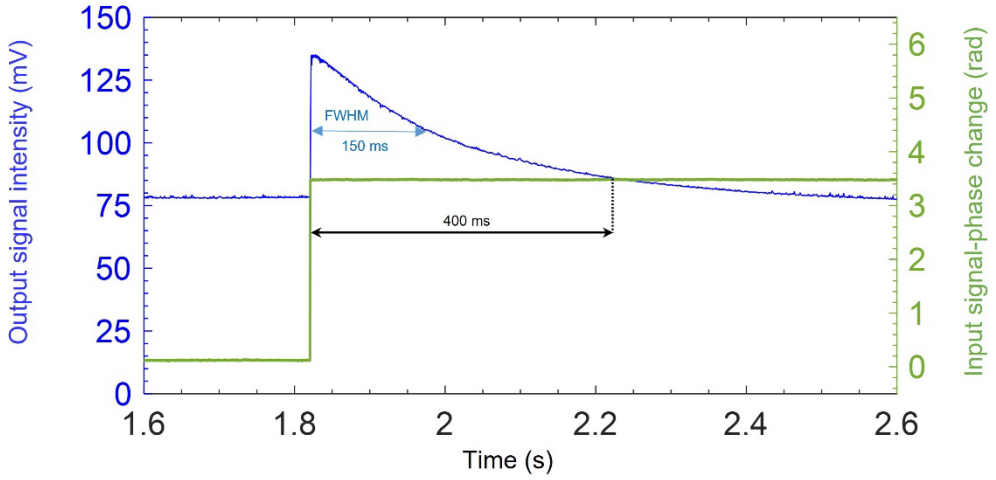


**Fig. 4.** Transient output signal measured on the photodetector (blue signal) and the applied phase change (green signal). Oscilloscope acquisition is set at 25 kS/s for 100 k points.

under blue TWM, according to the 400 ms obtained from Fig. 4. Note that output signal intensity shows a symmetrical response to the $2\pi$ ramp within the 25 ms, and a maximum value for a signal-phase change of $\pi$.

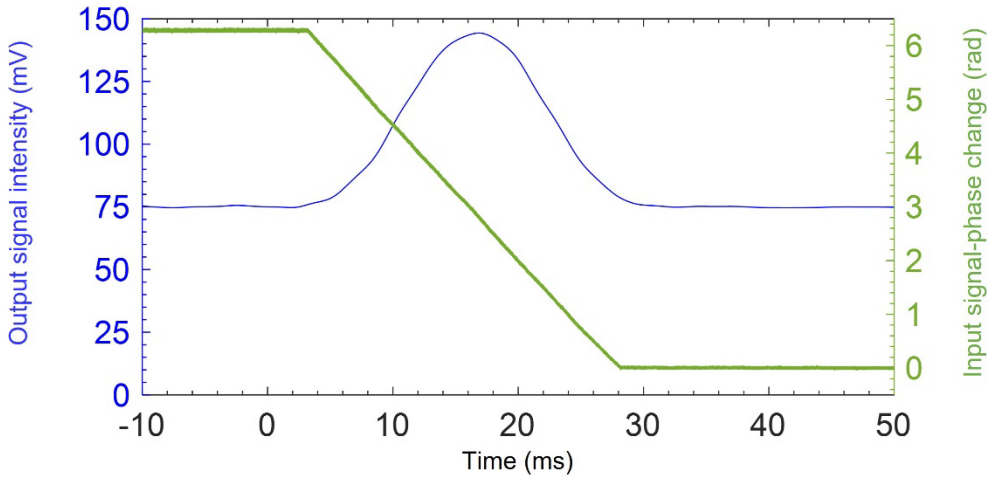


**Fig. 5.** Transient output signal measured on the photodetector (blue signal) and the applied signal-phase change (green signal). Oscilloscope acquisition is set at 2.5 MS/s for 1 M points.

Furthermore, Fig. 6 presents the measured OTD output signal depending on signal-phase change and the corresponding fit to Eq. (1), verifying the response of the system and effectiveness of the method. The maximum OTD signal is 67 mV, and the OTD signal for a signal-phase change of $\pi/2$ is 33.5 mV. Therefore, it is evident from these results that, using 100 times lower signal average input power, the OTD signal for the blue wavelength is 10 times higher than in our previous work [32], where femtosecond OTD was carried out in the infrared and subsequently the OTD signal was up-converted into the blue for detection. We must point out that experimental data in Fig. 6 are the main results of this work, because they provide the intensity-phase transfer

Optics EXPRESS

function which enables measurement of fast phase variations under a self-stabilized background. It means that any signal-phase change will give rise to an output signal which can be measured and, thus, the input signal-phase change can be inferred.

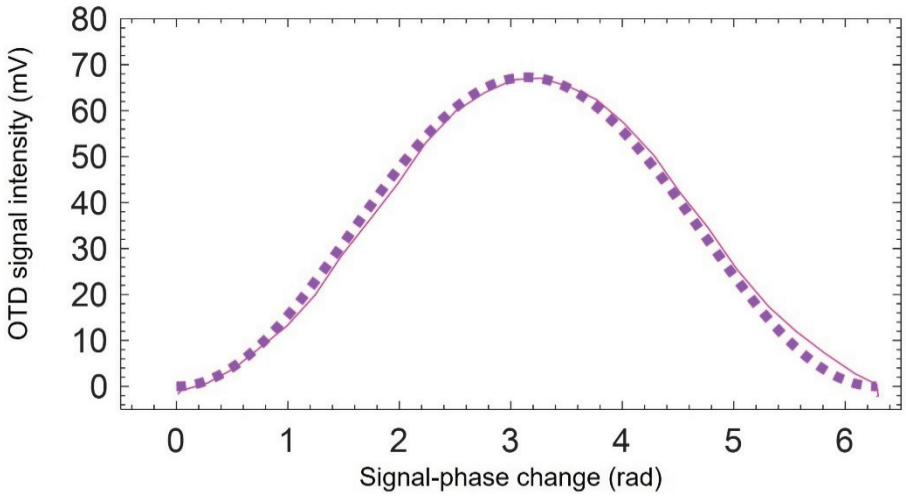


**Fig. 6.** OTD signal corresponding to applied signal-phase change. Plot contains experimental values (solid line), where background level $I^0$ of 75 mV has been subtracted according to the definition of the OTD signal intensity, $I^{OTD}$, as well as a fit (dashed line) to Eq. (1), $a_1 sin^2(\Delta\varphi/2)$, with $a_1 = 67 \pm 0.03$ and correlation factor $R = 0.993$.

In order to explore applications of our technique as an ultra-sensitive sensor, we analyze existing vibrations (non-self-stabilized) in our system and its amplified detection. Figure 7 displays the measured OTD output signals over 500 ms, for two different experimental conditions. Firstly, Fig. 7(a) shows the OTD output signal for the suppression state when no electronic signal is applied from the function generator, aiming to characterize natural vibrations existing in our environment. As can be seen from the left inset, there are temporal ranges where the OTD signal is flat at the bottom of the suppression state (with an average value of 77 mV and *std* of 0.1 mV), whereas the OTD signal shows some very small fast fluctuations for some temporal ranges within the 500 ms range. The right inset shows a magnified scale to see free-running phase fluctuations in our OTD signal, which are of the order of 2-3 mV. Secondly, we set our systems in a $\pi/2$ phase state, with respect to the stable background, in which the system should provide the maximum OTD signal for small phase changes, since the slope (32 mV rad$^{-1}$) in Fig. 6 is maximum at that point (well-known as a quadrature condition). Figure 7(b) presents the OTD output signal for the suppression state when applying a $\pi/2$ square-shaped pulse to the PZT mirror from the function generator (50 ms pulse duration, 5 ns rise/fall times), which is short compared to the response time of our photorefractive adaptive interferometer (400 ms). Given the repetition rate of our mode-locked pulse train of 76 MHz, corresponding to a pulse period of 13 ns, note that an electronic pulse of 50 ms affects some $3.8 \times 10^6$ mode-locked laser pulses. As soon as the $\pi/2$ phase pulse is applied on the input beam, the output shows a clear signal in intensity centered around 110 mV (corresponding to 34 mV at quadrature setpoint in Fig. 6) and fast intensity fluctuations with up to 15 mV peak-to-peak changes (see inset of Fig. 7 (b)), corresponding to small signal-phase variations $\leq 0.5$ *rad* as inferred from Fig. 6. Thus, intensity detection of vibrations in quadrature is magnified several times. After the electronic pulse, the OTD output reverts to the steady state, proving the self-adaptability and self-stability of the system.

Finally, we explore detection in the frequency domain by performing Fourier Transform analysis of temporal OTD signals. Figure 8 shows the corresponding Fourier transforms of

Optics EXPRESS

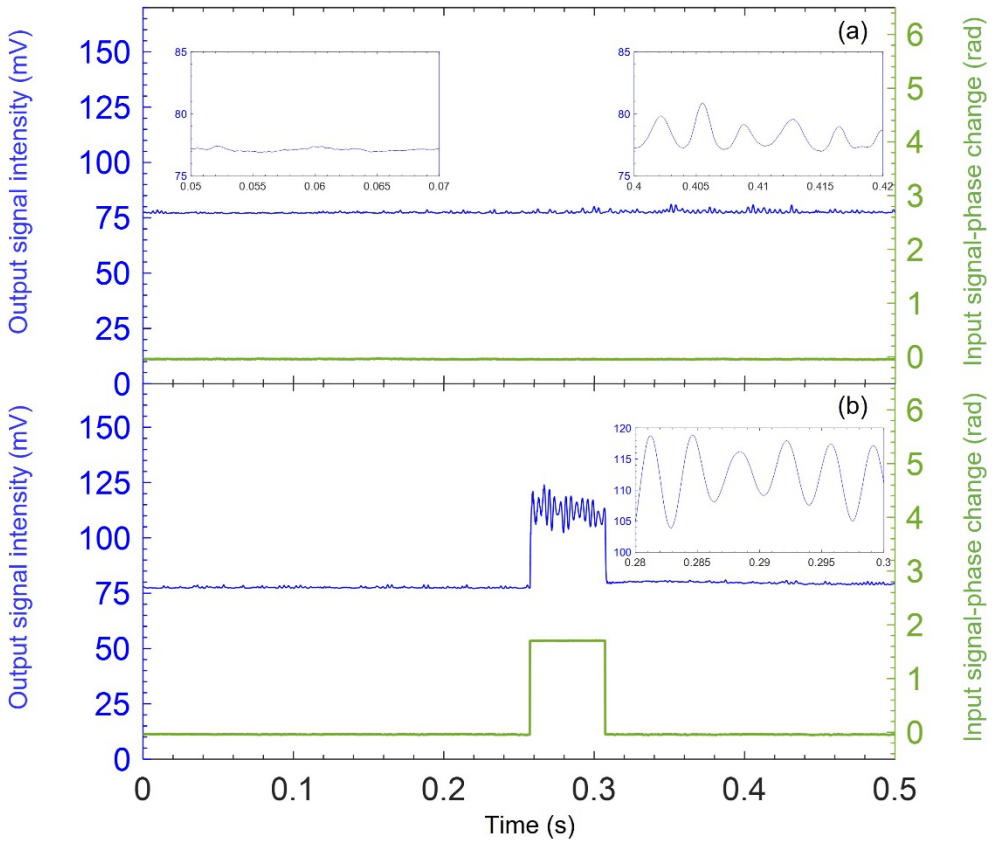


**Fig. 7.** (a) Transient output signal for free-running system, meaning that no electronic modulation is applied; (b) Transient output signal for an input signal pulse with squared-shape phase variation. Insets show zooms of regions of interest. Oscilloscope acquisition is set at 10 kS/s for 100 k points.

OTD signals for the different scenarios in Fig. 7. Firstly, Fig. 8(a) shows the spectrum of the free-running OTD signal (Fig. 7(a)) in which a very weak peak at 272 Hz is present. The absolute value of the amplitude at that peak is 635 a.u., with a relative spectral intensity (ratio between the squared-amplitude of a sideband of interest and the central peak) of $2.56 \cdot 10^{-6}$. That result confirms that the OTD signal is in suppression state and some very-weak fast-fluctuations are present. Regarding detection in quadrature, Fig. 8(b) shows the spectrum of Fig. 7(b) in which a peak at 272 Hz is clearly identified. The absolute value of the amplitude at that peak is 1676 a.u. with a relative spectral intensity of $1.68 \cdot 10^{-5}$. That result yields a spectral amplitude amplification factor of 2.6, corresponding to a spectral intensity amplification (by squaring absolute values of amplitudes) close to 7. It is worth pointing out that the spectrum of Fig. 7(b) contains a periodic modulation exactly at 20 Hz across the spectral range, as expected by the externally-injected 50 ms square-shaped pulse. These results quantify the significant enhancement of fast and weak signal-phase changes under the self-stabilized background.

Optics EXPRESS

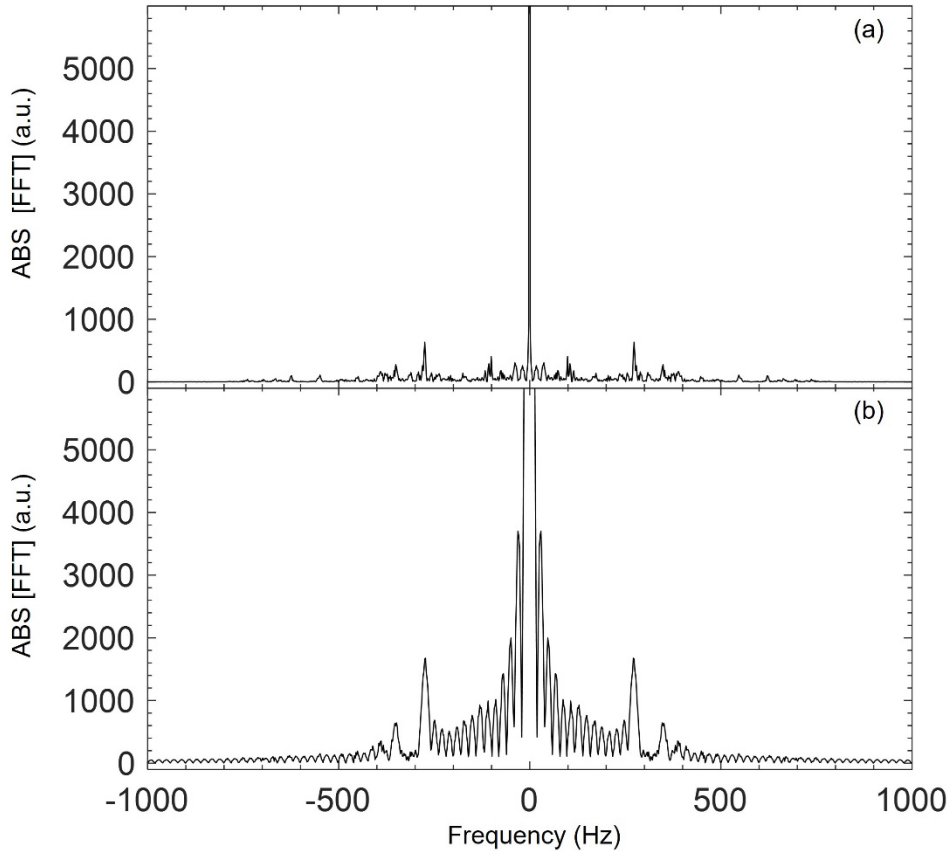


**Fig. 8.** Spectra of transient output signals in Fig. 7, for (a) free-running system and (b) for an input signal pulse with squared-shape phase variation. Note that vertical axes present absolute value (ABS) of the complex amplitude obtained by Fast Fourier Transform computation (FFT). Oscilloscope acquisition is set at 10 kS/s for 100 k points.

## 6. Analysis of results

In this section, we present additional information regarding the analysis of the experimental measurements in terms of frequency response, phase noise and signal-to-noise ratio (SNR), providing relevant information about the detection limits. It is worthwhile to clarify that this work is focused on demonstration of OTD using prior up-converted femtosecond pulses in the visible at high-repetition rates. While phase measurement records are not attempted, detection analysis is included for completeness.

As far as the temporal response of the adaptive system is concerned, the normalized frequency response of photorefractive effect can be defined as [43]:

$$\Delta I_N \equiv \frac{\Delta I}{\Delta I_{sat}} = \frac{2\pi f \tau_{sc}}{\sqrt{1 + (2\pi f \tau_{sc})^2}}, \tag{6}$$

where $\tau_{sc}$ is the time constant, $\Delta I$ is the intensity modulation, and $\Delta I_{sat}$ is the intensity modulation in saturation for high frequencies. The cutoff frequency, $f_c$, is defined as frequency at which $\Delta I_N = 0.5$, and thus, one can get the following relation $f_c = 1/\left(\sqrt{3}\ 2\pi\tau_{sc}\right)$.

Optics EXPRESS

The experimental time constant $\tau_{sc} = 150\,ms$ is estimated from the FWHM recovery time of the energy transfer after the application of the phase shift for a TWM interferometer (measured from Fig. 4), and corresponds to $f_c = 0.6\,Hz$. Figure 9 represents the numerical calculation of the temporal modulation transfer function, according to Eq. (6). Note that the dynamic hologram performs high-pass filtering of the signal during the phase-to-intensity transformation stage. Consequently, high-amplitude, low-frequency disturbance modulation does not affect the detection of small, high-frequency variations in the phase difference.

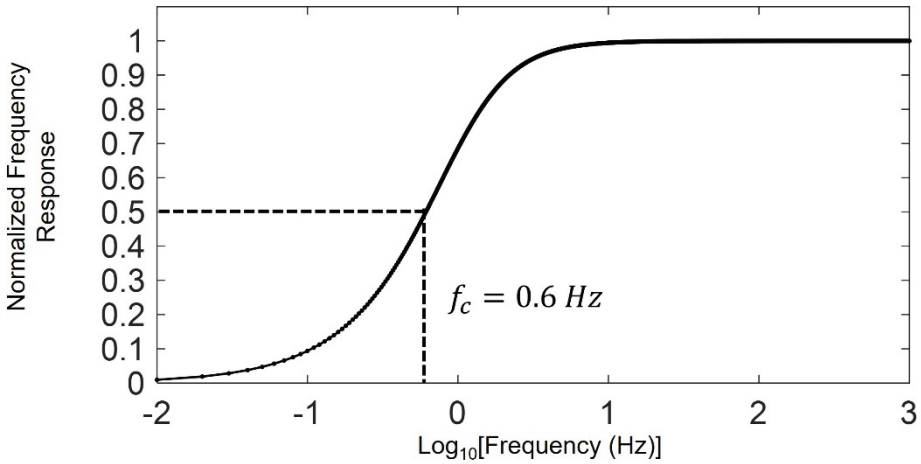


**Fig. 9.** Calculation of the normalized frequency response, according to Eq. (6), employing the experimental time constant $\tau_{sc}$ = 150 ms ($f_c$ = 0.6 Hz) measured in the TWM interferometer.

It should be noted from Fig. 9, that the frequency response nearly reaches its saturated value just at 10 Hz. Therefore, measurements of vibrations presented in Fig. 7 and Fig. 8, which are showing weak phase changes at frequencies beyond 200 Hz, are clearly performed far from the cutoff point.

Regarding the noise-equivalent phase of the system, Fig. 10 presents the experimental measurement of the minimal phase noise, when no phase modulation is applied to the signal beam. The noise-equivalent phase is obtained through the phase-intensity conversion provided by the calibration obtained from Fig. 6. This calibration allows converting the recorded signal noise to phase noise. We have to point out that the largest peak-to-peak phase changes are of the order of 0.1 rad, bearing in mind that no special isolation precautions to prevent and minimize fast fluctuations (such as air or mechanical vibrations, among others) have been implemented.

The importance of determining the phase noise spectral density (PNSD) is well known, as it provides information about detection limits based on the modulation frequency. Figure 11 presents the experimental measurement of the single-side PNSD in our system. As one can see, we identify a rise at low frequencies, as typically due to $1/f$ noise, as well as the noise floor given by the flat region, that starts above 1 kHz and provides a mean value of -70 dB, corresponding to $PNSD = 10^{-7}\mathrm{rad^2Hz^{-1}}$. The sensitivity of the interferometer provides critical insights into the noise characteristics of a system, its frequency-dependent performance, and its ability to detect angular signals. It is especially useful for assessing sensor quality, diagnosing issues, and optimizing designs for noise-sensitive applications. In our system, the sensitivity of the interferometer in terms of its phase noise, which defines the limit of the smallest detectable phase change in units of phase per root Hertz, will be $\sqrt{PNSD(\mathrm{rad^2Hz^{-1}})} = 3 \times 10^{-4}\ \mathrm{rad}/\sqrt{\mathrm{Hz}}$. That value of sensitivity is not significantly high, but typical of less-optimized interferometers, in which environmental fluctuation are not minimized.

Optics EXPRESS

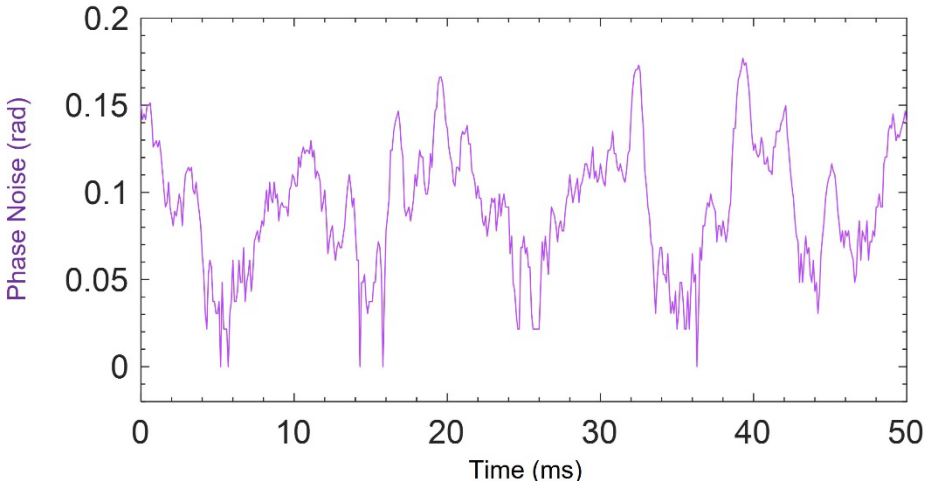


**Fig. 10.** Phase noise of the output signal measured on the photodetector in the absence of applied signal-phase change. Oscilloscope acquisition is set at 10 kS/s for 100 k points.

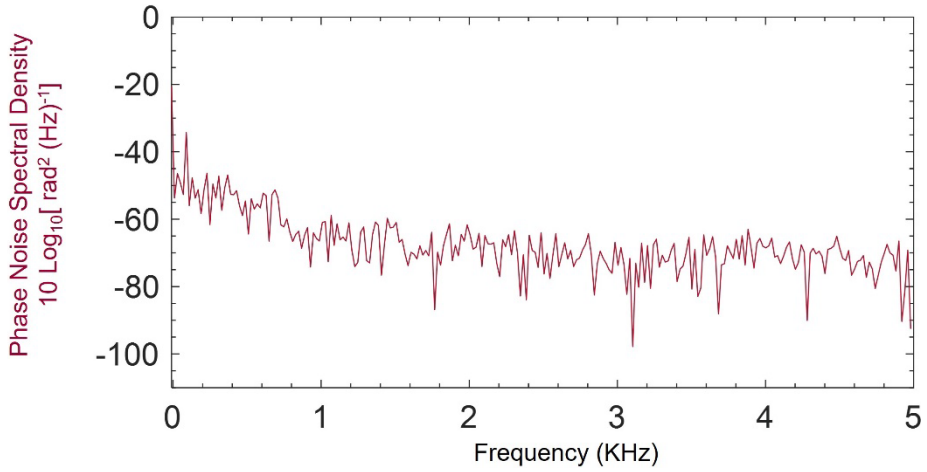


**Fig. 11.** Phase Noise Spectral Density of the output signal measured on the photodetector in the absence of applied signal-phase change. Note that vertical axes present the logarithmic value of the spectral density obtained by Fast Fourier Transform computation (FFT) of phase noise from Fig. 10. Oscilloscope bandwidth is 300 MHz.

Optics EXPRESS

In interferometry, the SNR determines the ability to discern weak signals from the background noise. Therefore, the ratio of a detectable phase change measured by an adaptive interferometer will be when signal is equal to noise, and this, a SNR larger than 1 will ensure clear detection. Low phase modulations, while reducing nonlinear distortions, pose challenges in maintaining adequate SNR. Piezo mirrors offer fine control over phase modulation, but their influence on SNR demands careful examination. At low phase modulations, the signal strength decreases, necessitating noise minimization to preserve SNR. Piezo mirrors provide stable and repeatable phase modulations, but thermal noise due to mechanical vibrations and electronic noise from the driver circuitry can dominate. Optimizing the driving electronics and isolating the system from environmental noise are crucial. SNR ratio of an adaptive interferometer can be experimentally estimated by computing the ratio of the summed squared magnitude of the signal to the summed squared magnitude of the noise, if the photo-detector's current is directly proportional to the optical power. Figure 12 present the SNR analysis of our weak-phase measurements from Fig. 7(b), where the average value of phase is 1.6 rad with a *std* of 0.1 rad (confirming the quadrature offset point). As we can see, SNR around 40 dB is achieved, confirming the clear detection of the peak center at 272 Hz, even under a noisy background.

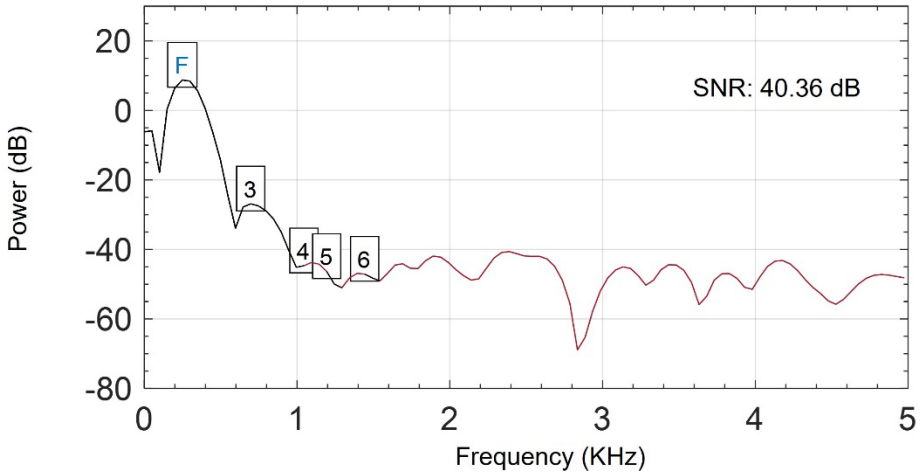


**Fig. 12.** Single-side power spectrum in dB of an oscillating input signal, sampled at a rate 10 KS/s. The computation of SNR identifies the fundamental (F) at 272 Hz and excludes the power contained in the lowest 6 harmonics, including the fundamental.

## 7. Conclusions

We have experimentally demonstrated, for the first time to our knowledge, the implementation of photorefractive two-wave-mixing using visible femtosecond pulses for background suppression and detection of transient optical phases in a photodetector. We have confirmed the relation between input and output phases for the entire range from 0 to $\pi$ applied to the visible beam, in agreement with squared-sinusoidal type theoretical dependence. The technique provides further background suppression with phase sensitivity using detection in the visible range, which is especially important for low-power small-phase change signals, and thus demonstrates its potential application as a sensor. The millisecond response time could be improved by using faster materials, such as semiconductors, while sensitivity could be increased by focusing beams and mitigating phase noise through environmental isolation. Nevertheless, we have demonstrated the use of this technique to detect weak and fast phase fluctuations by injecting a phase-triggering

Optics EXPRESS

signal, to set the system in quadrature condition, and enable enhanced signal-phase detection with SNR up to 40 dB.

It is worthwhile to highlight that the described technique allows probing samples at longer wavelengths, such as the near- or mid-infrared, and using photorefractive materials pumped in the visible, to allow detection at shorter wavelengths. Moreover, the demonstrated possibility of up-converting into the visible and performing OTD by efficient TWM could be extended to imaging, where CCD devices provide faster response with higher resolution.

Finally, we believe that this approach opens up new possibilities by exploiting unsurpassed wavelength flexibility for both sampling and detection, highlighting additional effects of blue-pump-synchronization in femtosecond OTD, such as low-average-power requirement, down to 1 mW at 76 MHz, for efficient background suppression.

**Funding.** Ministerio de Ciencia e Innovación (MCIN) (Alter PID2023-150006NB-I00, PID2020-120056GB-C22); MCIN/Agencia Estatal de Investigación (AEI) and European Union NextGenerationEU/PRTR (Ultrawave EUR2022-134051); Severo Ochoa Programme for Centres of Excellence in R&D (CEX2019-000910-S); Generalitat de Catalunya (CERCA); Fundación Cellex; FUNDACIÓ Privada MIR-PUIG; Department of Atomic Energy, Government of India (RTI 4007).

**Acknowledgments.** S. Chaitanya Kumar acknowledges the support of the Department of Atomic Energy, Government of India.

**Disclosures.** The authors declare no conflicts of interest.

**Data availability.** Data underlying the results presented in this paper are not publicly available at this time but may be obtained from the authors upon reasonable request.

## References

1. P. Yeh, *Introduction to Photorefractive Nonlinear Optics* (Wiley, 1993).
2. N. V. Kukhtarev, V. B. Markov, S. G. Odulov, *et al.*, "Holographic storage in electrooptic crystals.1. Steady-state," Ferroelectrics **22**(1), 949–960 (1978).
3. N. V. Kukhtarev, V. B. Markov, S. G. Odulov, *et al.*, "Holographic storage in electrooptic crystals.2. Beam coupling-light amplification," Ferroelectrics **22**(1), 961–964 (1978).
4. M. Cronin-Golomb, A. M. Biernacki, C. Lin, *et al.*, "Photorefractive time differentiation of coherent optical-images," Opt. Lett. **12**(12), 1029–1031 (1987).
5. D. Z. Anderson and J. Feinberg, "Optical novelty filters," IEEE J. Quantum Electron. **25**(3), 635–647 (1989).
6. R. S. Cudney, R. M. Pierce, and J. Feinberg, "The transient detection microscope," Nature **332**(6163), 424–426 (1988).
7. M. Woerdemann, F. Holtmann, and C. Denz, "Full-field particle velocimetry with a photorefractive optical novelty filter," Appl. Phys. Lett. **93**(2), 021108 (2008).
8. F. Holtmann, M. Oevermann, and C. Denz, "Dynamic phase-contrast stereoscopy for microflow velocimetry," Appl. Phys. B **95**(3), 633–636 (2009).
9. M. Sedlatschek, J. Trumpfheller, J. Hartmann, *et al.*, "Differentiation and subtraction of amplitude and phase images using a photorefractive novelty filter," Appl. Phys. B **68**(5), 1047–1054 (1999).
10. V. V. Krishnamachari and C. Denz, "Real-time phase measurement with a photorefractive novelty filter microscope," J. Opt. A: Pure Appl. Opt. **5**(5), S239–S243 (2003).
11. V. V. Krishnamachari, O. Grothe, H. Deitmar, *et al.*, "Novelty filtering with a photorefractive lithium-niobate crystal," Appl. Phys. Lett. **87**(7), 071105 (2005).
12. A. Esteban-Martín, J. García-Monreal, F. Silva, *et al.*, "Interferometric measurement of complex-field changes in transient detection imaging," Opt. Express **28**(20), 28782–28791 (2020).
13. I. Rossomakhin and S. Stepanov, "Linear adaptive interferometers via diffusion recording in cubic photorefractive crystals," Opt. Commun. **86**(2), 199–204 (1991).
14. A. A. Kamshilin, R. V. Romashko, and Y. N. Kulchin, "Adaptive interferometry with photorefractive crystals," J. Appl. Phys. **105**(3), 031101 (2009).
15. K. Shcherbin and M. B. Klein, "Adaptive interferometers with no external field using reflection gratings in CdTe:Ge at 1550 nm," Opt. Commun. **282**(13), 2580–2585 (2009).
16. M. B. Klein, "Beam coupling in undoped GaAs at 1.06 μm using the photorefractive effect," Opt. Lett. **9**(8), 350–352 (1984).
17. P. Delaye, A. Blouin, D. Drolet, *et al.*, "Detection of ultrasonic motion of a scattering surface by photorefractive InP:Fe under an applied dc field," J. Opt. Soc. Am. B **14**(7), 1723–1734 (1997).
18. F. M. Davidson and L. Boutsikaris, "Homodyne detection using photorefractive materials as beamsplitters," Opt. Eng. **29**(4), 369–377 (1990).
19. A. Blouin and J.-P. Monchalin, "Detection of ultrasonic motion of a scattering surface by two-wave mixing in a photorefractive GaAs crystal," Appl. Phys. Lett. **65**(8), 932–934 (1994).

Optics EXPRESS


20. R. K. Ing and J. P. Monchalin, "Broad-band optical-detection of ultrasound by 2-wave mixing in a photorefractive crystal," Appl. Phys. Lett. **59**(25), 3233–3235 (1991).
21. L. A. de Montmorillon, Ph. Delaye, and G. Roosen, "Photorefractive interferometer for ultrasound detection," in: K. Kuroda, ed., *Progress in Photorefractive Nonlinear Optics* (Taylor & Francis, 2002).
22. T. Sasaki, T. Yagami, T. Takashi, *et al.*, "Photorefractive flexoelectric liquid crystal mixtures and their application to laser ultrasonics," Opt. Mater. Express **13**(3), 728–738 (2023).
23. L. Peng, M. M. Varma, W. Cho, *et al.*, "Adaptive interferometry of protein on a BioCD," Appl. Opt. **46**(22), 5384–5395 (2007).
24. M. Ghotbi, M. Ebrahim-Zadeh, A. Majchrowski, *et al.*, "High-average-power femtosecond pulse generation in the blue using BiB3O6," Opt. Lett. **29**(21), 2530–2532 (2004).
25. M. Ghotbi, A. Esteban-Martin, and M. Ebrahim-Zadeh, "$BiB_3O_6$ femtosecond optical parametric oscillator," Opt. Lett. **31**(21), 3128–3130 (2006).
26. A. J. Torregrosa, E. Karamehmedovic, H. Maestre, *et al.*, "Up-Conversion sensing of 2D spatially-modulated infrared information-carrying beams with Si-based cameras," Sensors **20**(12), 3610 (2020).
27. A. S. Ashik, C. F. O'Donnell, S. Chaitanya Kumar, *et al.*, "Mid-infrared upconversion imaging using femtosecond pulses," Photonics Res. **7**(7), 783–791 (2019).
28. S. Junaid, S. Chaitanya Kumar, M. Mathez, *et al.*, "Video-rate, mid-infrared hyperspectral upconversion imaging," Optica **6**(6), 702–708 (2019).
29. X.-H. Chen, X.-F. Han, and Y.-X. Weng, "Transient spectrometer for near-IR fluorescence based on parametric frequency upconversion," Appl. Phys. Lett. **89**(6), 061127 (2006).
30. S. Cao, H. Li, Z. Zhao, *et al.*, "Ultrafast fluorescence spectroscopy via upconversion and its applications in biophysics," Molecules **26**(1), 211 (2021).
31. L. Peng, P. Yu, D. D. Nolte, *et al.*, "High-speed adaptive interferometer for optical coherence-domain reflectometry through turbid media," Opt. Lett. **28**(6), 396–398 (2003).
32. S. Sukeert, P.G. Chaitanya Kumar, Schunemann, *et al.*, "Up-converted photorefractive optical transient detection with femtosecond laser pulses," Opt. Express **31**(10), 16939–16951 (2023).
33. M. M. Kabir, D. Ito, Y. Oishi, *et al.*, "Two-wave mixing amplification of femtosecond laser pulses at 800 nm in Rh:$BaTiO_3$ photorefractive crystal," Jpn. J. Appl. Phys. **50**(10R), 102702 (2011).
34. L. H. Acioli, M. Ulman, E. P. Ippen, *et al.*, "Femtosecond temporal encoding in barium titanate," Opt. Lett. **16**(24), 1984–1986 (1991).
35. X. S. Yao, V. Dominic, and J. Feinberg, "Theory of beam coupling and pulse shaping of mode-locked laser pulses in a photorefractive crystal," J. Opt. Soc. Am. B **7**(12), 2347–2355 (1990).
36. M. Horowitz, B. Fischer, Y. Barad, *et al.*, "Photorefractive effect in a $BaTiO_3$ crystal at the 1.5-μm wavelength regime by two-photon absorption," Opt. Lett. **21**(15), 1120–1122 (1996).
37. B. A. Wechsler, M. B. Klein, C. C. Nelson, *et al.*, "Spectroscopic and photorefractive properties of infrared-sensitive rhodium-doped barium titanate," Opt. Lett. **19**(8), 536–538 (1994).
38. V. Dominic, X. S. Yao, R. M. Pierce, *et al.*, "Measuring the coherence length of mode-locked laser pulses in real time," Appl. Phys. Lett. **56**(6), 521–523 (1990).
39. G. C. Valley, "Short-pulse grating formation in photorefractive materials," IEEE J. Quantum Electron. **19**(11), 1637–1645 (1983).
40. H. Okamura, K. Takeuchi, T. Tanaka, *et al.*, "Grating formation with very short pulses in photorefractive materials: weak excitation limit," J. Opt. Soc. Am. B **14**(10), 2650–2656 (1997).
41. X. Yao and J. Feinberg, "Photorefractive pulse coupling in the frequency domain," Opt. Lett. **18**(2), 104–106 (1993).
42. M. Ghotbi and M. Ebrahim-Zadeh, "Optical second harmonic generation properties of $BiB_3O_6$," Opt. Express **12**(24), 6002–6019 (2004).
43. J. Frejlich, *Photorefractive Materials* (Wiley-Interscience, 2006).